ELSEVIER

International Journal of Mass Spectrometry 220 (2002) 1–10

International Journal of Mass Spectrometry

www.elsevier.com/locate/ijms

A G2(+) level investigation of the gas-phase identity nucleophilic substitution at neutral oxygen

Yi Ren [a,*], Joel L. Wolk [b], Shmaryahu Hoz [b]

[a] *School of Chemistry, Sichuan University, P.O. Box 73, Chengdu 610064, PR China*
[b] *Department of Chemistry, Bar-Ilan University, Ramat-Gan 52900, Israel*

Received 22 May 2002; accepted 6 June 2002

Abstract

G2(+) level molecular orbital calculations have been carried out for the identity nucleophilic substitution at saturated oxygen, $X^- + HOX \rightarrow HOX + X^-$ (X = F, Cl, Br, I). A comparison with data for the analogous reactions at saturated nitrogen, $X^- + NH_2X \rightarrow NH_2X + X^-$, and at saturated carbon, $X^- + CH_3X \rightarrow CH_3X + X^-$, indicate that the substitution reaction at saturated oxygen proceeds via a classic S_N2 pathway. The calculated intrinsic barriers $\Delta H^{\neq}_{cent}$ for substitution at oxygen are found to be much higher than the corresponding barriers for substitution at carbon and nitrogen, decreasing in the order F(106.3 kJ/mol) > Cl(92.5 kJ/mol) > Br(70.3 kJ/mol) > I(58.6 kJ/mol). Stabilization energies of the ion–molecule complexes decrease in the order F(187.9 kJ/mol) > Cl(97.5 kJ/mol) > Br(81.2 kJ/mol) > I(66.5 kJ/mol), that are also significantly higher than the corresponding values at carbon and nitrogen, and correlate well with the halogen electronegativities. The overall barriers relative to the reactants ($\Delta H^{\neq}_{ovr}$) are negative for all halogens F(−81.7 kJ/mol), Cl(−5.1 kJ/mol), Br(−10.7 kJ/mol), I(−8.1 kJ/mol). These trend is similar to that for the analogous reaction at nitrogen, but contrasts to that for the reactions at carbon where the $\Delta H^{\neq}_{ovr}$ are negative only for X = F. (Int J Mass Spectrom 220 (2002) 1–10)
© 2002 Elsevier Science B.V. All rights reserved.

Keywords: S_N2 at neutral oxygen; Ab initio calculation; Reaction mechanism

1. Introduction

The nucleophilic substitution reaction is a fundamental reaction which has played an important role in the development of modern physical chemistry [1]. Most theoretical and experimental investigations have been devoted to substitution at carbon atoms [2–7]. Recently interest has grown in substitution at non-stereogenic atoms—nitrogen [8–11], sulfur [12–15], oxygen [16,17], silicon [18–23] and phosphorus [24–28]. The paucity of studies of nucleophilic substitution at neutral oxygen [16,17] has stimulated our computational investigations of this kind of reaction.

Here, we report our high level ab initio calculations on nucleophilic substitution reactions at saturated oxygen in the gas phase. In particular, we investigate the reaction profile and the mechanism for identity nucleophilic reaction and compare the energy profiles with analogous reactions at saturated nitrogen and carbon atom.

2. Methods

Energy profiles for nucleophilic substitution reactions are very sensitive to the level of theory employed

* Corresponding author. E-mail: yiren57@sc.homeway.com.cn

1387-3806/02/$ – see front matter © 2002 Elsevier Science B.V. All rights reserved.
PII S1387-3806(02)00733-9

[29–33]. The G2(+) theory introduced by Radom and co-workers had been used successfully in theoretical studies of nucleophilic reactions at neutral carbon [3–5] and nitrogen [10] and appeared to be able reproduce quite well the experimental available data. In this paper we applied this method to the identity nucleophilic reactions at oxygen listed in following Eqs. (1)–(4):

$$F^- + HOF \rightarrow FOH + F^- \quad (1)$$

$$Cl^- + HOCl \rightarrow HOCl + Cl^- \quad (2)$$

$$Br^- + HOBr \rightarrow HOBr + Br^- \quad (3)$$

$$I^- + HOI \rightarrow HOI + I^- \quad (4)$$

All calculations were performed with the GAUSSIAN-98 package [34]. All electron (AE) calculation were done for first- and second-row atoms, while Wadt and Hay effective core potential (ECP) [35] were used for bromine and iodine—species, referred to as G2(+)-ECP. Full details of the basis set and procedures were presented elsewhere [36].

All reactant, ion–molecular complexes and transition state structures for reactions 1–4 were completely optimized at the HF/6-31+G(d) level first and re-optimized by MP2/6-31+G(d) with the frozen-core approximation. The nature of all optimized structure was determined using frequencies analysis at the HF/6-31+G(d) level. Charge distribution were obtained from the wave functions calculated at the MP2/6-311G(3df,2p) level on MP2/6-31+G(d) geometries, employing natural population analysis (NPA) [37–41]. Enthalpies at 298 K were derived using HF/6-31+G(d) harmonic frequencies scale by a factor of 0.8929 [42] and standard statistical thermodynamics formulas.

Throughout this paper, bond lengths are in angstroms, and bond angles are in degrees. Relative energies correspond to enthalpy changes at 0 K [ΔH (0 K)] or 298 K [ΔH (298 K)].

G2(+) total energies at 0 and 298 K of all species involved in reactions 1–4 are listed in Table 1.

Table 1
Calculated total energy (a.u.) for all species involved in the identity reaction X^- with HOX at 0 and 298 K

Species	G2(+) (0 K)	G2(+) (298 K)
F^-	−99.760599	−99.758239
HOF	−175.353358	−175.335683
$F^- \cdots HOF$	−275.185532	−275.167655
$[F^- \cdots HO \cdots F]^{-\neq}$	−275.145064	−275.126623
Cl^-	−459.808996	−459.80664
HOCl	−535.408543	−535.391786
$Cl^- \cdots HOCl$	−995.254637	−995.235052
$[Cl^- \cdots HO \cdots Cl]^{-\neq}$	−995.219470	−995.201751
Br^-	−13.229281	−13.226921
HOBr	−88.831103	−88.814764
$Br^- \cdots HOBr^-$	−102.09127	−102.07204
$[Br^- \cdots HO \cdots Br]^{-\neq}$	−102.06447	−102.04697
I^-	−11.446856	−11.444496
HOI	−87.057936	−87.041898
$I^- \cdots HOI$	−98.530183	−98.511149
$[I^- \cdots HO \cdots I]^{-\neq}$	−98.507859	−98.490501

3. Results and discussion

Our results show that the complete energy profile for gas-phase nucleophilic substitution at oxygen is described by a double-well potential curve (Fig. 1), analogues to those at carbon and nitrogen. The reaction involves an initial formation of a reactant ion–molecule complex **1**, with a complexation energy ΔH_{com} relative to the separated reactants. This complex must then overcome central activation barrier $\Delta H^{\neq}_{cent}$ to reach a symmetrical transition structure **2**. The latter then breaks down to give the product ion–molecule complex **1′**, finally dissociates into the separated products. The overall activation barrier relative to the separated reactants is denoted $\Delta H^{\neq}_{ovr}$.

Structures 1 and 2

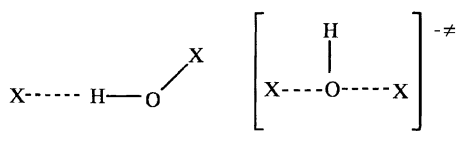

1 2

(a: X=F; b: X=Cl; c: X=Br; d: X=I)

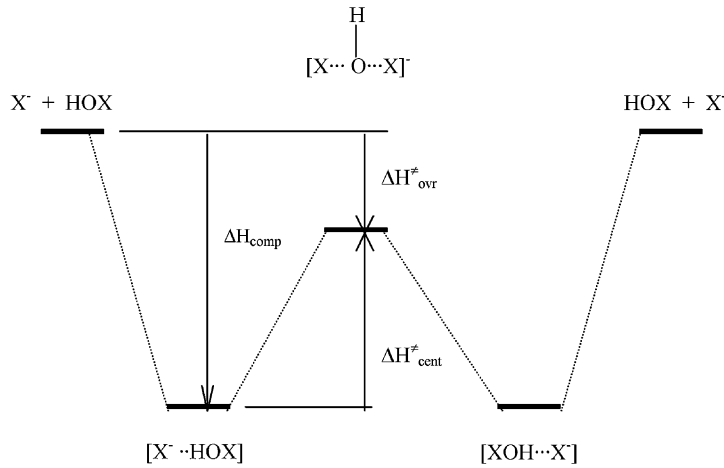

Fig. 1. Schematic potential energy surface for reactions 1–4.

3.1. Hypohalous acids HOX

The geometries of the hypohalous acids HOX are given in Table 2. Comparison of the calculated results for HOX (X = F, Cl, Br, I) with experimental structural data [43] shows reasonable agreement. The theoretical O–X bond lengths differ from the experimental values by up to 0.035 Å (for HOBr) while the largest deviation for the H–O bond lengths is 0.021 Å (for HOI). The calculated ∠H–O–X angles differ from experimental values by up to 2.9°. The largest relative error in all the theoretical values is less than 3%. The theoretical bond lengths of O–H in HOX are about 0.98 Å and the lengths of O–X bond increase considerably from HOF (1.454 Å) to HOI (2.019 Å).

Table 2
Geometrical parameters for reactants HOX (X = F, Cl, Br, I) at the MP2/6-31+G(d) level

Species	Level	*r*(H–O)	*r*(O–X)	∠(H–O–X)
HOF	MP2/6-31+G(d)	0.981	1.454	97.3
	Exptl. [43]	0.966	1.442	96.8
HOCl	MP2/6-31+G(d)	0.968	1.718	103.5
	Exptl. [43]	0.964	1.689	103.0
HOBr	MP2/6-31+G(d)-ECP	0.981	1.869	103.3
	Exptl. [43]	0.961	1.834	102.3
HOI	MP2/6-32+G(d)-ECP	0.981	2.019	105.3
	Exptl. [43]	0.960	1.959–1.995	102.4

NPA [44] shows that F atom in HOF bears a negative charge, and the X atoms in HOX (Cl, Br, I) bear a positive charge. The charge on the hydrogen atom changes modestly, the charge on the hydrogen atom in HOF being less positive than in other HOX. The negative charge on oxygen increases considerably from HOF to HOI.

3.2. Ion–molecule complexes

There are two conformers for the ion–molecule complexes. The first conformer takes the form of the halide anion complexing to the HOX through the hydrogen, whereas in the second conformation, the halide anion is in complexation through the halogen of HOX to form a so-called “X-philic” pre-reaction complex ($HOX\cdots X^-$). For the $Br^-\cdots HOBr$ species, Flowers and Francisco found that the minimum energy structure involves complexation with the hydrogen of the hypohalous acid. The total energy of $Br^-\cdots HOBr$ is lower than $Br^-\cdots BrOH$ by about 7.5 kJ/mol [45]. Therefore, X-philic complexes are not considered here.

Table 3
Geometrical parameters for ion–molecule complexes at the MP2/6-31+G(d) level in the identity reaction of X^- with HOX and relative elongation of the O–H bond (%O–H) due to complexation

Species	r(X–H)	r(H–O)	r(O–X)	∠(H–O–X)	%(O–H)
$F^-\cdots HOF$	1.212	1.173	1.474	101.0	19.6
$Cl^-\cdots HOCl$	1.961	1.026	1.708	104.6	4.7
$Br^-\cdots HOBr$	2.180	1.028	1.854	104.3	3.8
$I^-\cdots HOI$	2.421	1.011	2.001	105.3	3.1

3.2.1. Geometries

The calculated geometries of the complexes are presented in Table 3. The geometries of the HOX moieties in the $X^-\cdots HOX$ species differ from those of the unperturbed HOX molecules. The main changes are the elongation of the H–O bonds in the complex. The extent of elongation of the O–H bond can be measured by the parameter %O–H defined by the Eq. (5), where r^{comp}(O–H) and r^{react}(O–H) are the O–H bond lengths in the ion–molecule complex **1** and in the reactant HOX molecule, respectively,

$$\%O\text{–}H = \frac{100[r^{comp}(O\text{–}H) - r^{react}(O\text{–}H)]}{r^{react}(O\text{–}H)} \quad (5)$$

The %O–H values are direct proportional to the corresponding complexation energies ΔH_{comp}. There is a well defined linear relationship between %O–H and the ΔH_{comp} in $X^-\cdots HOX$ ($R^2 = 0.977$, Fig. 2).

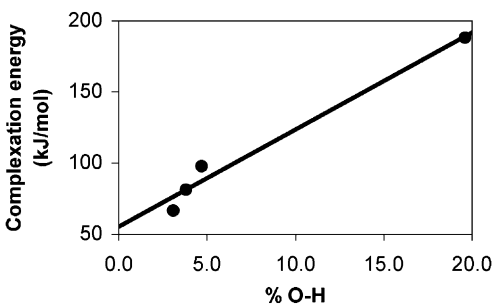

Fig. 2. Plot of G2(+) complexation energy (ΔH_{comp}, 0 K) of the ion–molecular complex **1** vs. the extent of elongation for bond O–H, denoted as %O–H. ΔH_{comp} values are listed in Table 5, %O–H values are listed in Table 3.

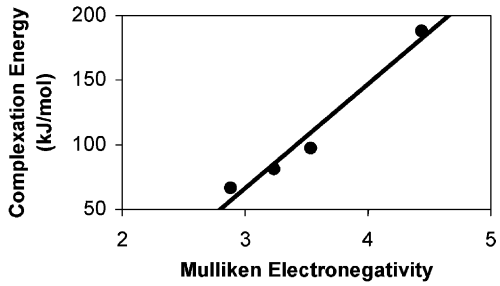

Fig. 3. Plot of G2(+) complexation energy (ΔH_{comp}, 0 K) of the ion–molecular complex **1** vs. the Mulliken electronegativities (in Pauling units, taken from [46]). ΔH_{comp} values are listed in Table 5.

3.2.2. Complexation energies

G2(+) complexation energies (ΔH_{comp}) for $X^-\cdots HOX$ are presented in Table 5 with corresponding values for the $X^-\cdots CH_3X$ and $X^-\cdots NH_2X$ complexes at the same level.

Our calculated complexation energies for $X^-\cdots HOX$ are greater than the corresponding ΔH_{comp} in $X^-\cdots CH_3X$ [3] and $X^-\cdots NH_2X$ [10]. This may be attributed to the greater electronegativity of oxygen atom in HOX, which renders the O–H group a more effective proton donor, leading to significant $X\cdots H\text{–}O$ hydrogen bonding in the $X^-\cdots HOX$ complexes. The complexation energies for $X^-\cdots HOX$ (X = F, Cl, Br, I) are found to decrease in the order, F(187.9 kJ/mol) > Cl(97.5 kJ/mol) > Br(81.2 kJ/mol > I(66.5 kJ/mol), which is also consistent with the basicity order in gas phase (F^- > Cl^- > Br^- > I^-).

The complexation energies for $X^-\cdots HOX$ (X = F, Cl, Br, I) show a good linear correlation with the halogen electronegativities using the Mulliken (R^2 = 0.986), Pauling (R^2 = 0.986) or Allred-Rochow (R^2 = 0.986) scale [46]. The correlation with the Mulliken scale is shown in Fig. 3. These correlation for the $X^-\cdots HOX$ (X = F, Cl, Br, I) complexes are analogous to those found for $X^-\cdots NH_2X$ [10] and $X^-\cdots CH_3X$ [3], although the complexation energies are much larger for $X^-\cdots HOX$ than for the corresponding $X^-\cdots NH_2X$ and $X^-\cdots CH_3X$. The larger complexation energies for $X^-\cdots HOX$ are consistent with the higher electronegativity of oxygen atom

Table 4
Geometrical parameters for transition state at the MP2/6-31 + G(d) level in the identity reaction of X^- with HOX and relative elongation of the O–X bond (%O–$X^{\neq}$)

	r(H–O)	r(O–X)	∠(H–O–X)	%(O–$X^{\neq}$)
$[F\cdots H\cdots OF]^{-\neq}$	0.968	1.766	84.4	9.8
$[Cl\cdots HO\cdots Cl]^{-\neq}$	0.979	2.109	89.4	23.5
$[Br\cdots HO\cdots Br]^{-\neq}$	0.984	2.237	91.0	20.7
$[I\cdots HO\cdots I]^{-\neq}$	0.989	2.381	94.4	19.0

in HOX, which renders the O–H group more effective proton donor, leading to significant $X^-\cdots$H–O hydrogen bonding in $X^-\cdots$HOX.

3.3. Transition state structures and barrier heights

G2(+) values for the central barriers $\Delta H^{\neq}_{cent}$ and overall barriers $\Delta H^{\neq}_{ovr}$ relative to separated reactants are included in Table 5. Geometries of the C_{2V} transition state structures are presented in Table 4.

3.3.1. Geometries

The TS structures at the G2(+) level of theory are found to have C_{2V} symmetry for $[X\cdots HO\cdots X]^{-\neq}$ (X = F, Cl, Br, I) similar to the transition structures $[X\cdots NH_2\cdots X]^{-\neq}$ [10] in the reaction $X^- + NH_2X$. The O–H bond lengths in the C_{2V} transition structures are found to be similar in magnitude, increasing marginally from 0.968 Å (**2a**) to 0.989 Å (**2d**). This behavior is similar to that of the N–H bond lengths in the C_{2V} transition structures for substitution at nitrogen [10] and the C–H bond lengths in the D_{3h} transition structures for substitution at carbon [3].

The main geometric feature in the transition structure is the elongation of the O–X bond relative to the ion–molecular complex. For S_N2 reactions at carbon [3] and nitrogen [10], the "looseness" of the transition state at the G2(+) level decreases in the order Cl > F > Br > I. The question arise whether this pattern exists between $\Delta H^{\neq}_{cent}$ of the oxygen species and transition state geometries in Table 4. We can readily characterize the looseness of the C_{2V} $[X\cdots HO\cdots X]^{-\neq}$ transition structures by a parameter %O–$X^{\neq}$: in a similar way to that proposed by Shaik et al. [2]:

$$\%O\text{–}X^{\neq} = \frac{100[r^{\neq}(O\text{–}X) - r^{comp}(O\text{–}X)]}{r^{comp}(O\text{–}X)} \quad (6)$$

where $r^{\neq}$(O–X) and r^{comp}(O–X) are the O–X bond lengths in the transition structure **2** and ion–molecular complex **1**, respectively. We find that %O–$X^{\neq}$ value for different X are close to one another and decrease in the order Cl > Br > F > I.

3.3.2. Barriers

Calculated central barriers $\Delta H^{\neq}_{cent}$ for the identity reactions $X^- + HOX \rightarrow HOX + X^-$ (X = F, Cl, Br, I) at the G2(+) level lie within a large range of about 48 kJ/mol, decreasing in the order F(106.3 kJ/mol) > Cl(92.5 kJ/mol) > Br(70.3 kJ/mol) > I(58.6 kcal/mol) at 0 K, which is significantly greater than corresponding barrier range in $X^- + H_2NX \rightarrow H_2NX + X^-$ (X = F, Cl, Br, I) (∼19 kJ/mol) and in $X^- + CH_3X \rightarrow CH_3X + X^-$ (X = F, Cl, Br, I) (∼13 kJ/mol) [10] (Table 5). The barrier heights $\Delta H^{\neq}_{cent}$ found in a smaller range for the $X^- + CH_3X$ reaction [3] can be explained by the fact that transition states involves the simultaneous making and breaking of the same bond. In the reaction $X^- + NH_2X$, a similar reactivity pattern is reproduced [10] even though the barrier range (48.8 ± 9.7 kJ/mol) at nitrogen is greater than the corresponding range at carbon (48.4 ± 7.1 kJ/mol). But this reactivity pattern breaks down for reaction $X^- + HOX \rightarrow HOX + X^-$, whose barrier heights $\Delta H^{\neq}_{cent}$ lie within a range of 47 kJ/mol (82.4 ± 23.8 kJ/mol). It seems that the barrier heights for halide exchange at oxygen are influenced by the nature of both the central atom and the halogen family.

The G2(+) overall barriers $\Delta H^{\neq}_{ovr}$ for $X^- + HOX$ are all negative analogous to the corresponding values for nitrogen, but in contrast to those for substitution at carbon [10] (Table 5), which are negative only for F, positive for X = Cl, Br and I [3], although general trends in the barrier patterns are similar (Table 5). The lower overall barrier are consistent with the larger complexation energies for $X^- + HOX$. Fluorine has the largest complexation

Table 5
Complexation energies (ΔH_{comp}) of the ion–molecule complexes, over all barrier heights relative to reactants ($\Delta H^{\neq}_{ovr}$) and central barriers ($\Delta H^{\neq}_{cent}$) for $X^- + HOX \rightarrow HOX + X^-$ reaction (kJ/mol)

X	ΔH_{comp}			$\Delta H^{\neq}_{ovr}$			$\Delta H^{\neq}_{cent}$		
	O	N[a]	C[b]	O	N[a]	C[b]	O	N[a]	C[b]
F	187.9	114.0	56.5	−81.7	−55.8	−8.0	106.3	58.2	48.5
	191.0		**57.1**	**−85.1**		**−11.0**	**105.9**		**46.1**
Cl	97.5	67.8	44.0	−5.1	−9.3	11.5	92.5	58.5	55.5
	99.8		**43.7**	**−7.2**		**9.8**	**92.7**		**53.5**
Br	81.2	58.4	41.5	−10.7	−13.7	5.8	70.3	44.7	46.9
	83.1		**40.0**	**−12.3**		**4.5**	**70.8**		**45.0**
I	66.5	50.0	36.0	−8.1	−10.8	6.5	58.6	39.1	42.5
	68.3		**35.3**	**−9.4**		**5.5**	**58.9**		**40.8**

Calculated energies at 298 K are given in bold.
[a] Values are corresponding energies for $X^- + NH_2X \rightarrow NH_2X + X^-$(G2(+)).
[b] Values are corresponding energies for $X^- + CH_3X \rightarrow CH_3X + X^-$(G2(+)).

energy (187.9 kJ/mol), which correlate with the lowest overall barrier (−81.7 kJ/mol). To our best knowledge, there is no experimental data available for the reactions $X^- + HOX$. Our theoretical studies suggest that gas-phase nucleophilic substitution reactions at neutral oxygen are energetically facile. However, it is possible that a following competitive proton transfer reaction may be favored:

$$X^- + HOX \rightarrow HX + OX^- \quad (7)$$

It has previously been found [43] that hypofluorous acid HOF is a slighter stronger acid than HF. Our G2(+) calculated reaction enthalpy predicts that the gas phase $F^- + HOF \rightarrow HF + OF^-$ reaction is exothermic, which means that deprotonation of HOF can compete significantly with S_N2 displacement. The other hyperhalous acids HOX are weaker than the corresponding hydrohalic acids HX (X = Cl, Br, I). Our calculation show that the $X^- + HOX \rightarrow HX + OX^-$ (X = Cl, Br, I) reaction are endotherrnic, which suggest that the deprotonation of these HOX are energetically unfavorable. Table 6 summarizes the calculated enthalpies for deprotonation reactions (Eq. (7)) at 0 and 298 K along with the corresponding experimental values at 298 K.

3.3.3. Charge distribution

Charge distributions in the transition state structures $[X\cdots HO\cdots X]^{-\neq}$ reveal a substantial positive charge on the OH moiety only for X = F [44]. This suggest a significant contribution of the triple ion valence bond configuration $F^-(OH)^+F^-$ in **2a**, similar to that found in the analogous reactions at nitrogen and carbon. This mixing of the triple ion configuration may be responsible for the stabilization of the transition state, leading to the lower $\Delta H^{\neq}_{ovr}$ for X = F. For the other halogens Cl and Br, the charges on the OH moiety are almost zero. For X = I, the negative charge of the OH

Table 6
Enthalpies of reactions $X^- + HOX \rightarrow HX + OX^-$ (kJ/mol)

	ΔH (0 K)	ΔH (298 K)	ΔH (298 K), exptl. [47]
$F^- + HOF \rightarrow HF + OF^-$	−44.9	−43.5	−37.8
$Cl^- + HOCl \rightarrow HCl + OCl^-$	89.7	91.2	93.0
$Br^- + HOBr \rightarrow HBr + OBr^-$	129.2	130.7	125.5
$I^- + HOI \rightarrow HI + OI^-$	154.8	156.1	165.0

moiety, as well as the smaller negative charge on the iodine atom ($q \approx -0.4e$) suggest that VB configuration $X(OH)^{-}X$ may override a reduced contribution of $X^{-}(OH)^{+}X^{-}$.

3.4. Correlation of $\Delta H^{\neq}_{cent}$ with energetic and geometrical characteristics of the transition state

There has been considerable discussion in the literature as to what factors might influence the barrier heights in gas-phase S_N2 reaction [3,5,10]. Here, we will briefly discuss our computational date for substitution at oxygen. We will seek the relationship between the central barrier and the geometrical and energetic characteristics of the transition state for substitution at oxygen, and check whether the reactions for substitution at oxygen show similar pattern of behavior to substitution at nitrogen and carbon.

3.4.1. Correlation of central barriers with reactant properties

In the previous study, a reasonable linear correlation was found between the central barrier at carbon and the gas-phase ionization energy value of X^{-}, IE(X^{-}), ($R^2 = 0.857$) [3], there is also a similar linear correlation at nitrogen ($R^2 = 0.896$) [10]. For the $X^{-} + HOX$ reaction such a correlation breaks down for F (Fig. 4), but there is still a definite linear correlation for Cl–I

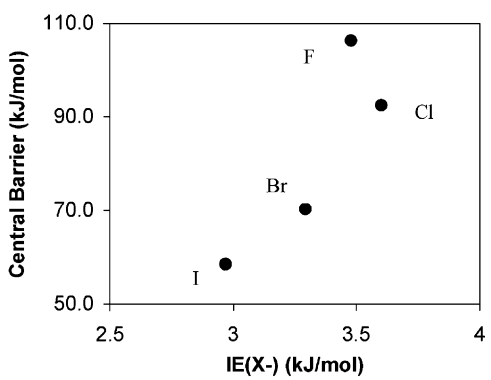

Fig. 4. Plot of G2(+) central barriers (ΔH_{cent}, 0 K) for substitution at oxygen vs. G2(+) gas-phase ionization energies of X^{-}(IE(X^{-})). G2(+) values of IE(X^{-}) are taken from Table 7, ΔH_{cent} values are listed in Table 5.

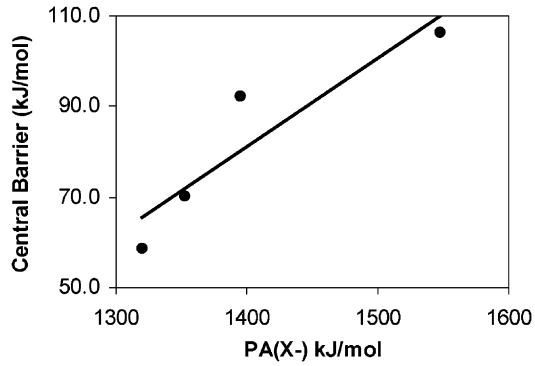

Fig. 5. Plot of G2(+) central barriers (ΔH_{cent}, 0 K) for reactions 1–4 vs. G2(+) proton affinities of X^{-}(PA(X^{-})). G2(+) values of PA(X^{-}) are taken from Table 7, ΔH_{cent} values are listed in Table 5.

($R^2 = 0.964$). Radom and coworkers found no linear correlation between the central barrier values and the proton affinity of X^{-}, PA(X^{-}), for halide substitution at carbon and nitrogen [3,10], but a reasonable correlation relation between the central barrier and PA(X^{-}) value exist for substitution at oxygen in our calculations ($R^2 = 0.8442$, Fig. 5).

We also checked whether there is a correlation between the central barrier and O–H dissociation energies $D_{O–X}$ in HOX. For substitution at carbon and nitrogen it was found that correlation between central barriers and bond dissociation energies $D_{C–X}$, $D_{N–X}$ fails for X = F, respectively. We found here that the correlation of central barrier at oxygen with the $D_{O–X}$ bond dissociation energies in HOX also fails for X = F (Fig. 6).

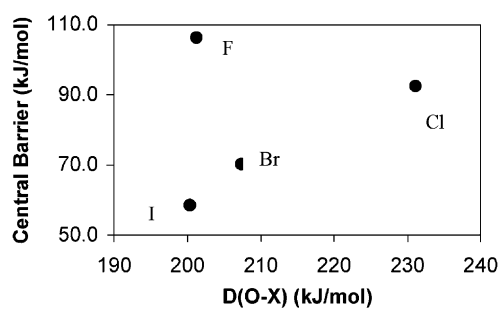

Fig. 6. Plot of G2(+) central barriers (ΔH_{cent}, 0 K) for reactions 1–4 vs. G2(+) dissociation energies of the O–X bond in HOX ($D_{O–X}$). $D_{O–X}$ values are taken from Table 8.

Table 7
Calculated G2(+) and experimental gas-phase proton affinity and ionization energies of X^-

X	PA(X^-) (kJ/mol)			IE(X^-) (eV)	
	G2(+), 0 K	G2(+), 298 K	Exptl. [47]	G2(+), 0 K	Exptl. [47]
F	1547.0	1550.7	1554.8	3.477	3.401
Cl	1394.6	1398.3	1395.0	3.602	3.614
Br	1352.7	1356.4	1353.5	3.293	3.364
I	1319.6	1323.3	1315.0	2.969	3.059

The calculated PA(X^-) and IE(X^-) are listed in Table 7. The dissociation energies $D_{O–X}$ are presented in Table 8.

3.4.2. Correlation of central barriers with the geometries of transition state

It was reported at the G2(+) level that there was a reasonable correlation between the central barrier and looseness of MP2 transition structure geometries for all halide substitution at carbon ($R^2 = 0.939$) [3] and at nitrogen ($R^2 = 0.887$) [10]. Our G2(+) results show that such a correlation is well for substitution at oxygen for X = Cl, Br, I ($R^2 = 0.999$), but fails for X = F (Fig. 7).

Thermodynamic looseness may be expressed by an index, $T^{\neq}$, analogous to that proposed by Shaik et al. [2] for substitution at carbon:

$$T^{\neq} = \frac{E_b(\mathrm{TS})}{D_{O–X}} \tag{8}$$

In Eq. (8), E_b(TS) is the binding energy of the transition state, defined by the following equation:

$$E_b(\mathrm{TS}) = E[X\cdots HO\cdots X]^{-\neq} - E(X^\bullet) - E(HO^\bullet) - E(X^-) \tag{9}$$

Table 8
Calculated G2(+) values of binding energies of transition structure E_b(TS) dissociation energies ($D_{O–X}$, 0 K) of the O–X bond in HO–X and the thermochemical looseness index $T^{\neq}$

X	E_b(TS)	$D_{O–X}$	$T^{\neq}$
F	282.9	201.2	1.41
Cl	236.2	231.1	1.02
Br	218.0	207.3	1.05
I	208.4	200.3	1.04

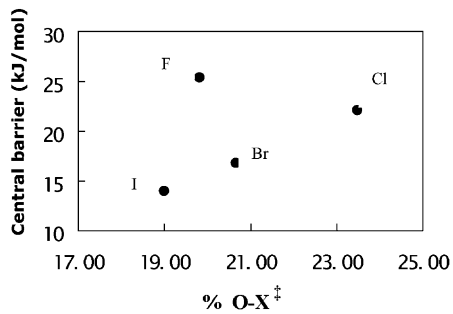

Fig. 7. Plot of G2(+) central barriers (ΔH_{cent}, 0 K) for reactions 1–4 vs. the central barrier geometric looseness index (%O–$X^{\neq}$, see Eq. (6)). The G2(+) values of %O–X are presented in Table 4.

In the present study, we find no correlation between $T^{\neq}$ and $\Delta H^{\neq}_{cent}$, $T^{\neq}$ and %O–X. These results are similar to those found for substitution at carbon and nitrogen [3,10].

In above discussion, we find the fluorine behaves in many respects different than the other halogens. This phenomena may imply the deprotonation (Eq. (7), X = F) instead of displacement reaction (Eq. (1)) is perhaps the best "candidate" for observation in the gas phase, as judged from energetic consideration (Table 6).

4. Conclusions

The identity exchange reaction at the saturated oxygen atom $X^- + HOX \rightarrow HOX + X^-$ were investigated at the G2(+) level of ab initio theory, leading to following conclusions:

1. The energy profile for the gas-phase reactions is described by a double-well curve which is a

classical S_N2 mechanism. The following pathway for the model reaction is established:

$$X^- + HOX \rightarrow X^- \cdots HOX \rightarrow [X \cdots HO \cdots X]^{-\neq} \rightarrow XOH \cdots X^- \rightarrow HOX + X^-$$

2. Central barrier energies $\Delta H^{\neq}_{cent}$ for substitution at oxygen for X = F ∼ I spans a range of 47.7 kJ/mol, much larger than the range of 19.4 kJ/mol for substitution at nitrogen and 13.0 kJ/mol for substitution at carbon. The barriers decrease in the order F(106.3 kJ/mol) > Cl(92.5 kJ/mol) > Br(70.3 kJ/mol) > I(58.6 kJ/mol). $\Delta H^{\neq}_{cent}$ for substitution at oxygen are significantly higher than that for substitution at nitrogen and carbon, which indicates that the central barrier heights are significantly affected by the nature of central atom and the atom undergoing attack.
3. The overall barrier $\Delta H^{\neq}_{ovr}$ for $X^- + HOX \rightarrow HOX + X^-$ are negative for all halogens that is similar to the corresponding values for nitrogen, but in contrast with those for carbon, where the barrier $\Delta H^{\neq}_{ovr}$ is negative only for F. Our results suggest that nucleophilic substitution reaction at oxygen are likely to be relatively facile process in the gas phase and will take place more readily than at carbon.
4. Complexation energies ΔH_{comp} decrease in the order F(187.9 kJ/mol) > Cl(97.5 kJ/mol) > Br(81.2 kJ/mol) > I(66.5 kJ/mol). These values are larger than those found for the corresponding nitrogen complexes and carbon complexes. The complexation energies of the $X^- \cdots HOX$ complexes are found to correlate with halogen electronegativity and the elongation parameter %O–H.
5. The correlation between G2(+) central barrier for substitution at oxygen with the geometrical looseness of the transition state breaks down for F. There is no correlation between the central barrier and thermodynamical looseness. The central barriers correlate reasonably with the proton affinity PA(X^-).

Acknowledgements

This work was supported by the Barbara and Kort Sino-Israel Post-Doctoral Fellowship Program.

References

[1] T.H. Lowry, K.S. Richardson, Mechanism and Theory in Organic Chemistry, 3rd Edition, Harper & Row, New York, 1987.
[2] S. Shaik, H.B. Schlegel, S. Wolfe, Theoretical Aspects of Physical Organic Chemistry, The S_N2 mechanism, Wiley, New York, 1992.
[3] M.N. Glukhovtsev, A. Pross, L. Radom, J. Am. Chem. Soc. 117 (1995) 2024.
[4] M.N. Glukhovtsev, A. Pross, L. Radom, J. Am. Chem. Soc. 118 (1996) 6273.
[5] M.N. Glukhovtsev, A. Pross, H.B. Schlegel, R.D. Bach, L. Radom, J. Am. Chem. Soc. 118 (1996) 11258.
[6] M.N. Glukhovtsev, R.D. Bach, A. Pross, L. Radom, Chem. Phys. Lett. 260 (1996) 558.
[7] E. Uggerud, J. Chem. Soc., Perkin Trans. II (1999) 1459.
[8] M. Bühl, H.F. Schaefer III, J. Am. Chem. Soc. 115 (1993) 9143.
[9] R.M. Minyaev, D.J. Wales, J. Phys. Chem. 98 (1994) 7942.
[10] M.N. Glukhovtsev, A. Pross, L. Radom, J. Am. Chem. Soc. 117 (1995) 9012.
[11] R. Gareyev, S. Kato, V.M. Bierbaum, J. Am. Soc. Mass Spectrom. 12 (2001) 139.
[12] S.M. Bachrach, D.C. Mullhearn, J. Phys. Chem. 100 (1996) 3535.
[13] D.C. Mullhearn, S.M. Bachrach, J. Am. Chem. Soc. 118 (1996) 9415.
[14] B.D. Gailbreath, C.A. Pommerening, S.M. Bachrach, L.S. Sunderlin, J. Phys. Chem. 104 (2000) 2958.
[15] S.M. Bachrach, B.D. Gailbreath, J. Org. Chem. 66 (2001) 2005.
[16] P. Beak, J. Li, J. Am. Chem. Soc. 108 (1986) 3834.
[17] S.M. Bachrach, J. Org. Chem. 55 (1990) 1016.
[18] L.P. Davis, L.W. Burggraf, M.S. Gordon, K.K. Baldridge, J. Am. Chem. Soc. 107 (1985) 4415.
[19] R. Damrauer, L.W. Burggraf, L.P. Davis, M.S. Gordon, J. Am. Chem. Soc. 110 (1988) 6601.
[20] J.A. Deiters, R.R. Holmes, J. Am. Chem. Soc. 109 (1987) 1686.
[21] S. Gronert, R. Glaser, A. Streitwieser, J. Am. Chem. Soc. 111 (1989) 3111.
[22] U. Brandemark, E.M. Siegbahn, Theoret. Chem. Acta 66 (1984) 233.
[23] R.R. Holmes, Chem. Rev. 90 (1990) 17.
[24] E.P. Kyba, J. Am. Chem. Soc. 97 (1975) 2554.
[25] E.P. Kyba, J. Am. Chem. Soc. 98 (1976) 4805.
[26] J. Nielsen, O. Dahl, J. Chem. Soc., Perkin. Trans. II (1984) 553.

[27] S.M. Bachrach, D.C. Mullhearn, J. Phys. Chem. 97 (1993) 12229.
[28] M.B. Tollefson, J. Li, P. Beak, J. Am. Chem. Soc. 118 (1996) 9052.
[29] Y.J. Cho, L.S.R. Vande, L. Zhu, W.L. Hase, J. Chem. Phys. 96 (1992) 8275.
[30] Z. Shi, R.J. Boyd, J. Am. Chem. Soc. 113 (1991) 1072.
[31] S. Shaik, A. Ioffe, A.C. Reddy, A. Pross, J. Am. Chem. Soc. 116 (1994) 262.
[32] W.-P. Hu, D.G. Truhlar, J. Phys. Chem. 98 (1994) 1049.
[33] B.D. Wladkowski, J.I. Brauman, J. Phys. Chem. 97 (1993) 13158.
[34] M.J. Frisch, G.W. Trucks, H.B. Schlegel, G.E. Scuseria, M.A. Robb, J.R. Cheeseman, V.G. Zakrzewski, J.A. Montgomery, R.E. Stratrmann Jr., J.C. Burant, S. Dapprich, J.M. Millam, A.D. Daniels, K.N. Kudin, M.C. Strain, O. Farkas, J. Tomasi, V. Barone, M. Cossi, R. Cammi, B. Mennucci, C. Pomelli, C. Adamo, S. Clifford, J. Ochterski, G.A. Petersson, P.Y. Ayala, Q. Cui, K. Morokuma, D.K. Malick, A.D. Rabuck, K. Raghavachari, J.B. Foresman, J. Cioslowski, J.V. Ortiz, B.B. Stefanov, G. Liu, A. Liashenko, P. Piskorz, I. Komaromi, R. Gomperts, R.L. Martin, D.J. Fox, T. Keith, M.A. Al-Laham, C.Y. Peng, A. Nanayakkara, C. Gonzalez, M. Challacombe, P.M.W. Gill, B. Johnson, W. Chen, M.W. Wong, J.L. Andres, C. Gonzalez, M. Head-Gordon, E.S. Replogle, J.A. Pople, GAUSSIAN 98, Revision A.7, Gaussian, Inc., Pittsburgh, PA, 1998.
[35] W.R. Wadt, P.J. Hay, J. Chem. Phys. 82 (1985) 284.
[36] M.N. Glukhovtsev, A. Pross, M.P. McGrath, L. Radom, J. Chem. Phys. 103 (1995) 1878.
[37] A.E. Reed, R.B. Weinstock, F. Weinhold, J. Chem. Phys. 83 (1985) 735.
[38] J.F. Carpenter, F. Weinhold, J. Mol. Struct. (Theochem.) 169 (1988) 41.
[39] F. Weinhold, J.E. Carpenter, The Structure of Small Molecular and Ions, Plenum Press, New York, 1988, p. 227.
[40] A.E. Reed, F. Weinhold, Isr. J. Chem. 21 (1991) 277.
[41] A.E. Reed, L.A. Curtiss, F. Weinhold, Chem. Rev. 88 (1988) 899.
[42] L.A. Curtiss, K. Raghavachari, G.W. Trucks, J.A. Pople, J. Chem. Phys. 94 (1991) 7221.
[43] M.N. Glukhovtsev, A. Pross, L. Radom, J. Phys. Chem. 100 (1996) 3498.
[44] Calculated NPA charges are available as supporting information (Tables S1–S3).
[45] B.A. Flowers, J.S. Francisco, J. Phys. Chem. A 105 (2001) 494.
[46] L.C. Allen, J. Am. Chem. Soc. 111 (1989) 9003.
[47] NIST Standard Reference Database Number 69, July 2001 Release (http://webbook.nist.gov/chemistry).